Draft: The effect of methane-ammonia and methane-hydrogen blends on ignition and light-around in an annular combustor

Yi Hao Kwah* [a], Samuel Wiseman [b], James R. Dawson [a]

[a]Department of Energy and Process Engineering,
Norwegian University of Science and Technology
Trondheim, Norway

[b]SINTEF Energy Research AS
Trondheim, Norway

July 29, 2024

Abstract

The use of hydrogen and ammonia in gas turbines, either alone or blended with natural gas, poses various technical challenges for combustion systems, including ignition. Depending on the fuel composition, the laminar flame speed and the ratio of unburned to burned gas density (dilatation ratio) of hydrogen and ammonia flames can be well outside the range seen in natural gas flames. Previous studies in annular combustion chambers have provided evidence of the importance of these properties in determining the ignition dynamics including light around times. So far, these studies have mostly considered hydrocarbon fuels, have been limited to only a few runs, and have not yet systematically investigated variations in the dilatation ratio and the flame speed but rather have considered them as a lumped parameter. To investigate these effects in more detail, experiments characterizing the light around times were carried out on an atmospheric annular combustor in which the dilatation ratio and the laminar flame speed was independently varied. This was achieved by varying the equivalence ratio and employing a variety of different hydrocarbon fuels (ethylene, propane, methane) and fuel blends of methane-ammonia and methane-hydrogen. Light around times were evaluated from global chemiluminescence measurements obtained using an azimuthal array of photomultipliers placed round the combustor chamber as well as high speed imaging. To improve statistical certainty, more than 3000 ignition and light-around times were measured with 30 repetitions obtained for each operating condition. To provide some insight into the light around dynamics in specific cases, 900 of the 3000 sets included high-speed OH chemiluminescence images. Light around times for premixed pure hydrocarbon flames showed a similar dependence on S_L as reported in previous studies . For the range of ammonia fuel blends investigated, an increase in laminar flame speed leads to a predictable increase in the flame propagation speed, as in the case of hydrocarbon fuel. Furthermore, collapse of this dependence for all blends could be achieved when corrected for an effective Lewis number, noting that all Lewis numbers for these blends were above unity. However, for hydrogen fuel blends, a decrease in dilatation ratio was found to decrease the light-around time counter to existing experimental results on the ignition of hydrocarbon fuels for which we currently do not have an explanation.*

1 INTRODUCTION

Unlike ignition and stabilisation of a flame on an individual injector, ignition in an annular combustor

*Address all correspondence to this author.

which has a uniform distribution of circumferentially arranged injectors is more complex as the ignition and stabilisation of a flame on one injector is followed by the ignition and stabilisation of flames on all the other injectors in a process known as light-around. Light-around is characterised by the successful formation of a flame kernel at the spark location leading to the ignition of one injector and spreads as two propagating flame fronts one in the clockwise and one in the anti-clockwise direction igniting each injector before finally merging approximately 180° away from the initial flame kernel location. The characteristic time-scale for the successful ignition of all injectors in an annular combustor is referred to as light-around time. Investigations into premixed combustors using gaseous hydrocarbon fuels have so far pointed to key mechanisms affecting the absolute flame propagation speed, dynamics and stochastic aspects of light around which are: (1) laminar flame speed S_{L}, (2) ratio of the upstream unburned gas density to the downstream burnt gas density, known as the dilatation ratio $\rho_{\mathrm{u}}/\rho_{\mathrm{b}}$, and (3) turbulence effects.

Due to the unusual properties of ammonia-air and hydrogen-air flames, it is not clear whether correlations developed in previous studies of light-around are applicable for fuel blends containing these fuels. Stoichiometric methane-air mixtures have flame speeds of 0.35 m/s whereas ammonia-air mixtures have speeds of only 0.07 m/s. On the other hand, the flame speed of hydrogen-air is an order of magnitude larger at 2.3 m/s. Furthermore, a hydrogen-air mixture with the same laminar flame speed as a stoichiometric methane-air mixture has a dilatation ratio that is only about half of that of a methane-air flame. Previous correlations have not been tested at these extremes.

In the first study of light around by Bourgouin et al. [1], the laminar flame speed S_L was identified as a key parameter in determining the light-around time and was supported by Prieur et al [2] in spray flames who also observed a first order dependence of the flame propagation speed on S_{L}. Using a similar combustor geometry, Xia et al. [3] also found a dependence between S_{L} and the light around time. Ciardiello et al. [4] considered pure CH_4 and C_2H_4 when matching S_{L} = 0.24, 0.30, and 0.36 m/s across different operating points. They found that for the same laminar flame speed, the ignition light-around time was almost identical and therefore independent of the fuel. The authors reasonably concluded that S_{L} exerted a first order influence on the flame propagation speed and proposed that the flame propagation is largely controlled by S_{L}, and is more dominant than dilatation effects. In all these studies, hydrocarbon fuels were used which limits the range of laminar flame speed that could be achieved by varying the equivalence ratio, ϕ. As such, identifying the relative contributions of $\rho_{\mathrm{u}}/\rho_{\mathrm{b}}$ and S_{L} in flame propagation for lean premixed hydrocarbon fuel-air mixtures presents a challenge. However, this can be achieved using fuel blends of methane-ammonia, methane-hydrogen, and methane-ammonia-hydrogen.

Using the dilatation ratio, the density ratio of cold unburnt gaseous reactants ρ_{u} to hot burnt gas products ρ_{b} across a flame front, to scale the flame propagation speed was proposed by Ruetsch et al. [5]. In annular and multi-injector combustion systems, $\rho_{\mathrm{u}}/\rho_{\mathrm{b}}$ is often reported [1, 2, 4, 6, 7], but its contribution to flame propagation/light around has been generally qualitative. This is because changing ϕ changes both $\rho_{\mathrm{u}}/\rho_{\mathrm{b}}$ and S_{L} simultaneously in pure hydrocarbon-air flames. A recent Large Eddy Simulation (LES) study performed by Töpperwein et al. [8] on the MICCA annular combustor has provided detailed insight into the effect of $\rho_{\mathrm{u}}/\rho_{\mathrm{b}}$. The evolution of $\rho_{\mathrm{u}}/\rho_{\mathrm{b}}$ during light-around showed that the volumetric expansion of hot burnt gases leads to an increase in azimuthal flow velocity of up to 400% during the initial light-around process greatly enhancing the azimuthal flame propagation speed. A peak flame speed was observed to occur around a quarter through the light-around phase, followed by a gradual decay due to the continual increase in ρ_{b} value (and thus, a decrease in $\rho_{\mathrm{u}}/\rho_{\mathrm{b}}$) as the freshly burnt gases are continually cooled by the cold combustor walls.

Turbulence can also have a significant effect on the ignition process by enhancing the flame speed. Many turbulent flame speed studies have been performed in spherical fan-stirred bombs summarised in the review papers of [9, 10]. Various proposed correlations exist for S_{T}, such as the empirical ones from Bradley et

al. [11], Kobayashi et al. [12], and the analytical equations of Zimont [13], and have been utilised in annular ignition studies of Bourgouin et al. [1], Xia et al. [3], and Zhong et al. [14]. In general, there is reasonably good agreement between the fitted S_T equations and the measured propagation speeds in annular combustors which may be due to the similarities of flame kernel formation and expansion in spherical bombs and the present annulus geometry [1]. However, uncertainties remain as to whether turbulent flame speed correlations from fan-stirred bombs are generally applicable to annular combustion chambers which contain varying regions of high shear and recirculation zones depending on the number of injectors [15, 16].

Ignition studies have also focused on the impact of injector spacing in both annular and linear combustor arrays. Barré et al. [6] performed a parametric investigation in which a linear multi-injector array was configured to have l_s/d_{inj}= [4.5, 13] with l_s being the separation distance between adjacent injectors and d_{inj} as the injector exit diameter. It was found that for $l_s/d_{inj} \leq 8$, the swirling flame rapidly propagates via a spanwise mechanism while larger values of l_s/d_{inj} results in a slower, and more stochastic axial propagation mode. Ciardiello et al. [4] observed a mixed propagation mechanism (axial and spanwise azimuthal mode) for a 12-injector and 18-injector annular configuration, which corresponds to l_s/d_{inj} = 2.34 and 1.56 respectively[1]. The reported ignition times suggested minimal impact of injector spacing on propagation speed, at least in the range of l_s/d_{inj} values considered.

This paper investigates the ignition dynamics and light around times for a variety of different hydrocarbon fuels (ethylene, propane, methane) and fuel blends of methane-ammonia and methane-hydrogen in the annular combustor at NTNU operating under atmospheric conditions and in premixed mode. Using different combinations of these fuel blends and varying the equivalence ratio, the dilatation ratio and the laminar flame speed could be independently varied to isolate their component contributions. Injector spacing is also further examined to complement previous investigations by Machover and Mastorakos [7,17] and Ciardiello et al [4], to gain new insights on how it influences ignition dynamics. A large number of experiments were carried out (over 3000) as each experimental condition was repeated a minimum of 30 times. Next, the experimental procedure and operating conditions are presented which is followed by a presentation and discussion of the results.

[1]In an annular configuration, l_s refers to the arc distance between adjacent injectors.

2 EXPERIMENTAL SETUP

2.1 The annular combustor

In the current study, two different geometric configurations of the NTNU atmospheric annular combustor (Fig. 1) are considered:

(1) a 6-injector combustor in which flames are stabilised by means of a bluff body with the injector geometry shown in the inset of Fig. 1.

(2) A 12-injector with the same bluff body configuration.

The current work was conducted using bluff-body stabilised flames in order to minimise flow complexity and because bluff-body stabilised flames are more resistant to flash back than swirling flames when operating with hydrogen. The 6-injector bluff body stabilised flames is taken to be the reference geometric case where the bulk of experiments are conducted. It has a larger injector-to-injector spacing of l_s/d_{inj} = 4.67, where l_s is the arc distance between injectors and d_{inj} is the injector exit diameter, compared to the typical 12-injector (l_s/d_{inj} = 2.34) used in previous studies of the Cambridge/NTNU combustor [18, 19]. This results in relatively large recirculation zones where the gas velocities and velocity gradients are significantly lower than near the injectors. The movement of flame front is better resolved in these regions and changes in the propagation velocity around the chamber can be measured more accurately. There is also a better isolation of the flame propagation dynamics, minimising the effect of any flame interaction between injectors as the flame kernel travels around the annulus. In both configurations, the inner and outer combustor walls are of the same height at 200 mm, since it was pointed out in [8] that the mass outflow of burnt gases is an important parameter affecting flame propagation. A quartz sec-

tion of 50 mm is placed on the outer combustor wall for optical access. The short quartz height captures the full stabilised flame but limits the field of view and serves to block high intensities from the spark ignitor avoiding saturation in the PMTs and intensified cameras. The spark electrode is positioned 55 mm above the combustor dump plane, mid-point between injector sectors I-1 and I1 as depicted in Fig. 2. To minimise any potential flow disruption, the electrode tip is almost flush with the inner combustor wall. The spark is powered via a Danfoss EB14 transformer, identical to that used in [1,20]. Continuous sparks of 50 mJ are produced every 20 ms.

2.2 Diagnostics and measurements

To characterise the light around times and dynamics, several diagnostic approaches were used simultaneously. To quantify the light-around timescales, an azimuthal array of six Hamamatsu H11902-13 photomultipliers (PMTs) with a spectral response of 185 to 700 nm were fitted with UV filters centred at (310 ± 10) nm. A schematic of the PMT array is shown in Fig. 2. These provided line-of-sight 1D time-series of the global heat release sampled at 51.2 kHz. Extension tubes and slits with adjustable apertures were used to adjust the field-of-view (FoV) at each injector. The FoV at the injector exit mid-plane was kept constant at 26.6 mm for the minor axis, and 54.9 mm for the major axis. Two high-speed Phantom V2012 cameras each equipped with a LaVision High-Speed Intensified Relay Optics unit and a UV filter centred at (310 ± 10) nm were used to image the flames at 10 kHz from both the side and overhead via an air-cooled mirror as shown in Fig. 1.

2.3 Ignition procedure

The ignition procedure used in all the experiments was as follows: (1) The combustor was cooled to room temperature to ensure that the thermal state at ignition was repeatable and minimise additional variability in the light-around process [8,21,22]. It also ensured that comparisons could be made with other studies. (2) The combustion chamber was filled with the premixed reactants for 5 s to ensure a homogeneous volume of gasses when ignition occurred noting that the residence time is approximately 1.25 s for 6-injector configuration under cold flow conditions when the injector exit velocity U = 4 m/s, . (3) The transformer was then triggered for 0.5 s to produce multiple sparks, with each spark duration at about 7.5 ms. It was observed that in all instances of the 910 runs for which high-speed imaging was recorded, the successful light-around always originated from a flame kernel at a single time instant, and not flame kernels formed at different time instants. For each operating condition, at least 30 runs are performed to ensure a good statistical convergence so that reliable conclusions may be drawn concerning the stochastic behaviour of ignition light-around behaviour [7].

2.4 Operating conditions

Table 1 summarises the different fuels used and key combustion properties obtained from laminar flame calculations using Cantera [26] over a range of operating conditions. The injector exit velocity is kept constant at U = 10 m/s for all cases. Ignition and light-around times for conventional hydrocarbon gases, ethylene (C_2H_4) and propane (C_3H_8) were tested as baseline cases to compare with the literature. As done in previous experiments [2–4,7], the equivalence ratio is changed to observe the dependence of light around times. Changing the equivalence ratio alters both S_L and ρ_u/ρ_b which form a lumped parameter that can be considered an approximation of the absolute flame propagation speed in the absence of turbulence.

In an effort to isolate the component effects of S_L and ρ_u/ρ_b, different fuel blends of CH_4 with H_2 and/or NH_3 were used. The fixed quantities are highlighted in blue in Table 1.

1. To isolate the effect of varying ρ_u/ρ_b, blends of CH_4-H_2 were used to fix S_L at ≈ 0.35 m/s by adjusting the H_2 volume fraction and equivalence ratio. This enabled ρ_u/ρ_b to be varied between 4.10 to 7.51.
2. To isolate the effect of varying S_L, blends of CH_4-NH_3 were adjusted to keep ρ_u/ρ_b approximately constant ($\approx$ 7.39 to 7.51). S_L was varied by adjusting the blend ratios and equivalence ratio. In some cases, H_2 was added at 5% or 10% of the total reactant flow rate volume fraction to the blends of CH_4-NH_3 to further increase the range

Table 1: Table of operating conditions. Flame properties which are kept constant are highlighted in blue.

Fuel (blends)	Chem mechanism	S_L [m/s]	ρ_u/ρ_b [-]	$(\rho_u/\rho_b)\cdot S_L$ [m/s]	Le_{eff} [-]	ϕ [-]
Cases for comparing effect of $(\rho_u/\rho_b)\cdot S_L$						
C_2H_4	Wang [23]	[0.347 to 0.685]	[6.85 to 8.43]	[2.38 to 5.77]	[1.15 to 1.27]	[0.70 to 1.16]
C_3H_8	Qin [24]	[0.329 to 0.409]	[7.63 to 8.25]	[2.51 to 3.38]	[1.37 to 1.54]	[0.87 to 1.09]
Cases for comparing effect of ρ_u/ρ_b						
CH_4-H_2	Sandiego [25]	0.342±3.54%	[4.64 to 7.51]	[1.53 to 2.59]	[0.61 to 1.04]	[0.44 to 0.95]
Cases for comparing effect of S_L						
CH_4-H_2	Sandiego	[0.345 to 0.687]	7.51	[2.59 to 5.15]	[1.04 to 1.20]	[0.95 to 1.08]
CH_4-NH_3	Sandiego	[0.109 to 0.345]	7.44±0.90%	[1.21 to 2.59]	[1.03 to 1.04]	[0.95 to 0.98]
CH_4-NH_3–H_2	Sandiego	[0.164 to 0.687]	7.39±2.43%	[2.66 to 5.15]	[1.11 to 1.40]	[0.95 to 1.08]

of S_L up to 0.69 m/s.

2.5 Estimation of an effective Lewis Number

As both NH_3 and H_2 were used, the effect of preferential diffusion on flame propagation and therefore the light around times was considered. To estimate an effective Lewis number, a two-reactant approach is adopted [27]. This involves computing the Lewis number for both the fuel (Le_F) and the oxidiser (Le_O). Since multi-component fuel blends are used, a weighted Le_F is constructed. Although there is no agreed approach to characterising the Le of multi-component mixtures, two main approaches can be adopted [28]: (1) volume-based [29], or (2) heat release (mass)-based [30].

The volumetric weighted expression, defined in Equation 1 below, has been used to provide qualitative estimates of L_{eff} and Markstein lengths $\mathcal{M}$ with reasonable confidence for H_2-C_xH_y blends at moderate turbulent intensities [28].

$$Le_F = \sum_{i=1}^{N} x_i Le_i, \quad \sum_{i=1}^{N} x_i = 1 \text{ for } i = 1^{st}, ..., N^{th} \text{ fuel species} \tag{1}$$

where x_i refers to the mole fraction of each fuel species and Le_i is the Lewis number of the i^{th} fuel species.

The heat release approach proposed by Law et al. [30] has been applied to premixed reactants composed of 3 different fuels [31,32] and is defined as:

$$Le_F = 1 + \frac{\sum_{i=1}^{N} q_i^* (Le_i - 1)}{\sum_{i=1}^{N} q_i^*} \quad \text{for } i = 1^{st}, ..., N^{th} \text{ fuel species} \tag{2}$$

where q^* is the normalised heat release rate evaluated by:

$$q_i^* = \frac{QY_i}{c_p T_u} \tag{3}$$

where Q is the heat of reaction (kJ/kg), Y_i is the species mass fraction (upstream), c_p is the heat capacity of the mixture (kJ/(kg K)), and T_u is the unburned mixture temperature (K).

These approaches allow us to estimate an effective Lewis number Le_{eff} following the approach of others [28,33–35]:

$$Le_{eff} = 1 + \frac{(Le_E - 1) + (Le_D - 1)\cdot \mathcal{A}}{1 + \mathcal{A}} \tag{4}$$

Here, Le_D refers to the Lewis number of the deficient reactant which is the fuel under lean premixed conditions, thus $Le_D = Le_F$ and Le_E for the excess reactant. The parameters $\mathcal{A}$, Φ and β are defined

as [36,37]:

$$\mathcal{A} = 1 + \beta(\Phi - 1) \tag{5}$$

$$\Phi = \begin{cases} \frac{1}{\phi}, & \text{if } \phi < 1 \\ \phi, & \text{otherwise} \end{cases} \tag{6}$$

$$\beta = \frac{E}{\mathcal{R}} \frac{(T_b - T_u)}{T_b^2}, \qquad \text{where } \frac{E}{\mathcal{R}} = -2 \frac{\mathrm{d}\ln(\rho_u S_L)}{\mathrm{d}(1/T_b)} \tag{7}$$

where $\mathcal{A}$ is a measure of the strength of the reactant mixture, Φ is a parameter related to the equivalence ratio defined to be ≥ 1, β is the Zel'dovich number, a dimensionless activation energy, E is the activation energy, $\mathcal{R}$ is the universal gas constant, and T_b is the burned gas temperature. To the best of the authors' knowledge no empirical data exist for the Le for NH_3 and H_2 blends used in this study.

Fig. 3a plots the Le_{eff} for a fixed ρ_u/ρ_b for a range of CH_4-NH_3 mixtures with 0%, 5%, and 10% H_2 enrichment by volume (the corresponding values of ϕ are reported in the caption). Estimates of Le_{eff} using both the volume fraction or heat-release (mass) fraction methods are shown in black and red respectively. Using the heat release based method shows a significant increase in the Le_{eff} for different levels of H_2 enrichment, from $Le_{\text{eff}} = 1.05$ to 1.4, compared with the small changes using the volume based method. However, for all volume fractions of $NH_3 > 0$, fixing ρ_u/ρ_b results in an approximately constant Le_{eff}. Fig. 3b plots Le_{eff} for a fixed S_L (achieved by decreasing ϕ) for a range of CH_4-H_2 mixtures from 0 – 100% H_2 by volume (values of ϕ are reported in the caption). The heat release based method shows little change in Le_{eff} up to 60% H_2 volume fraction which is expected as the corresponding change in mass is minimal. On the other hand, a quasi-linear decrease in Le_{eff} is predicted using the volume based method. Overall, the figures indicate that fixing ρ_u/ρ_b also fixes the Le_{eff} for the CH_4-NH_3 blends investigated, which enables the effect of S_L on the light around times to be isolated. However, fixing S_L using different CH_4-H_2 blends results in variation in Le_{eff} which needs to be taken into account when evaluating the light around times due to its impact on the flame propagation speed (as will be shown in Fig. 7).

3 Results

3.1 Determination of light around times

Two methods were used to determine the light-around times. The first method used an azimuthal array of PMTs which measure the 1-D time-series of the global heat release rate of the flame as it propagates around the annulus and can be used to evaluate global time-scales. The second method was high speed OH* chemiluminescence imaging from overhead which provides line-of-sight imaging of the flame as it propagates around the annulus and can be used to evaluate global time-scales as well as provide insight into the dynamics of flame propagation around the annulus. The 1-D PMT signals cannot provide detailed insight into the spatial evolution of flame propagation around the annulus but can provide global information with a spatial resolution determined by the FoV of the PMTs. By dividing the annular chamber into sectors according to the number of injectors, the time delay between ignition of the first and last injector could then be determined by an intensity threshold as shown in Fig. 4. High-speed imaging was performed for 900 of the 3000 experimental runs. The flame propagation speed can also be evaluated from these high speed chemiluminescence images and is discussed in the next section.

Using the PMT time-series data, the light-around time is defined as the characteristic time-delay between the first and last PMT that detects 15% of the normalised maximum OH* intensity as illustrated in Fig. 4. The same approach was used in [20] and is similar to the threshold approach used in [38]. In [38], the threshold chosen was the maximum detected OH* emissions between adjacent PMTs. It is important to note that although there is some arbitrariness to the choice of threshold, there is good repeatability in the light-around times.

Fig. 4 shows typical PMT data of a light-around sequence in the 6-injector configuration. The blue lines correspond to PMTs viewing injectors in the clockwise direction and the red lines in the anti-clockwise direction as denoted in Fig. 2. The figure shows that ignition of each injector is characterised by a slow increase in heat release rate which then rapidly grows

and spikes before levelling off to a constant value. The chosen threshold in these experiments is shown by the shaded grey region, which is once the rapid growth in heat release has started. The figure also shows the light-around time, denoted by the arrow τ_{ign}, which can also be evaluated for both the CW and ACW branches.

Fig. 5 shows two typical light around sequences viewed from overhead for the 6 and 12 injector configurations. In the 6 injector configuration (top), the CW flame branch propagates slightly faster than the ACW flame branch. As the flame reaches each burner, a peak in the intensity occurs (circular regions of bright orange/yellow) which corresponds to the peak observed in the PMT time-series data. This is due to the volume of gas above the injector being ignited. The flame then stabilises which is shown by a reduction in intensity to lower but constant values on average. This process is illustrated by the injector $I5$ which is circled in white. It is important to note that the light-around time is defined as the characteristic time it takes for the flame to propagate around the annulus and not the time taken to achieve flame stabilisation which would be the time taken for the OH* signal to reach steady state conditions. A reference start time is taken as the successful ignition of the first injector as used in [8, 38] and not the formation of the initial flame kernel which has been shown in previous studies to have considerable variability [2,8,38,39]. The averaged (absolute) propagation speed, $\overline{S}_{\mathrm{a}}$ is then computed in the same manner as [4] by assuming that each flame branch travels approximately half the annulus circumference. This approach is relatively robust as the vast majority of light-around sequences show that the CW and ACW flame branches merge near the mid-point. Variations in the merging point occur when the initial flame kernel and early stages of propagation lead to the ignition of $I1$ ahead of $I-1$ as seen in Fig. 5. This results in one of the flame branches leading the other.

3.2 Estimating the flame propagation speed

Estimates of the absolute flame propagation speed, S_a, can be obtained using either the PMT data or the high speed OH* imaging. To compare the two approaches, several tests were run using three different operating conditions which were: CH_4(40%) – NH_3(60%) blend at ϕ = 0.97, CH_4 at ϕ = 0.95, and H_2 at ϕ = 0.44. For each blend, S_{a} was estimated by dividing half the circumference by the measured ignition time and taking the average over 45 runs with the PMT data and 10 runs from the imaging data. The results are presented in Table 2.

Table 2: Summary of the flame propagation speed S_{a} computed using 1-D PMT signals and 2-D integrated OH* overhead images. The difference in speed from the different methods is shown as $|\Delta S_{\mathrm{a}}|$. All speeds are reported in m/s.

Fuel mixture	ϕ	S_{a}(PMT)	S_{a}(Image)	$\lvert\Delta S_{\mathrm{a}}\rvert$
CH_4 (40%)-NH_3 (60%)	0.97	2.35	3.45	1.10
CH_4	0.95	5.52	6.53	1.01
H_2	0.44	6.76	7.85	1.09

The relative change in values estimated from both sets of data, S_a(PMT) and S_a(Image), are equally consistent as illustrated by the fact that $|\Delta S_{\mathrm{a}}| \approx 1$. This means that estimating the absolute value of S_a is a challenge but both methods provide a robust reference velocity to identify the dependence of light around time and propagation speed on the laminar flame speed and dilation ratio for different fuel blends. For purposes of statistical convergence we therefore use S_a(PMT) as the reference method. However, the imaging data will be used to ensure we only compare ignition sequences which originated from a single spark instant and discard spurious runs.

3.3 Effect of laminar flame speed

The correlation between S_{a} and S_{L} is plotted in Fig. 6 for the pure hydrocarbon fuels ethylene and propane. In these experiments, varying ϕ varies both $\rho_{\mathrm{u}}/\rho_{\mathrm{b}}$ and S_{L} as a lumped parameter. Reasonably good collapse is found. The strong linear correlation between S_{a} and $(\rho_{\mathrm{u}}/\rho_{\mathrm{b}}) \cdot S_{\mathrm{L}}$ is consistent with previous studies [2–4].

To investigate the effect of S_{L} on S_{a}, a series of CH_4-NH_3 blends with increasing NH_3 volume fractions are used to fix $\rho_{\mathrm{u}}/\rho_{\mathrm{b}}$. A wide range of S_{L} is achieved by varying the equivalence ratio and the ad-

dition of H_2 as listed in Table 1.

Fig. 7 plots the variation of S_a with S_L for CH_4-NH_3-H_2 blends and varying Le_{eff} corrections. Fig. 7a corresponds to no Le_{eff} correction whereas Fig. 7b and Fig. 7c correspond to Le_{eff} corrections by volume and heat release rate respectively. Overall, the values of S_a show a linear decrease with the product of ρ_u/ρ_b and S_L for mixtures with increasing volume fraction of NH_3. This is consistent with the expectation that increasing NH_3 volume fraction decreases S_L. This linear dependence is maintained for fixed levels of H_2 volume fraction of 5% to 10%. However, when both ρ_u/ρ_b and S_L are fixed, small increases in the H_2 volume fraction increase S_a as shown by the approximately uniform offset. This suggests that the inclusion of H_2 increases the flame propagation speed during light around.

Thermo-diffusive effects have yet to be considered in light-around studies since most studies have considered pure hydrocarbon fuels. Furthermore, as noted by Lancien et al. [38], the effects of local curvature and Markstein length $\mathcal{M}$, Lewis number Le, and Zel'dovich number β, on flame propagation are usually of an order of magnitude lower than turbulent flame speed effects. However, measurement of turbulent flame speeds in fan-stirred bombs have demonstrated significant impacts of thermo-diffusive effects [9,10,27]. Therefore, due to the highly thermo-diffusive nature of H_2, an attempt to scale S_a with an effective Le_{eff} was made using the Le_{eff} definitions described in Section 2.5.

Plots including the Le_{eff} determined by the volumetric and heat release rate methods are plotted in Fig. 7b and Fig. 7c respectively. Incorporating Le_{eff} using the volume-based approach makes little difference. However, it is evident that an Le_{eff} computed using the heat release approach scales S_a with $(\rho_u/\rho_b)\cdot S_L \cdot Le_{eff}$ for all blends with 5% and 10% H_2 enrichment by total air-fuel volume. Overall, a very good collapse is achieved and it is worth noting that the Le_{eff} are greater than unity for all of these operating points. This suggests that the Lewis number effects significantly influence the flame propagation speed in the case of fuel blends containing H_2. However, blends without H_2 still exhibit a constant offset and the authors do not currently have an explanation for this. Although it is worth mentioning that there is no agreed consensus on the formulation of Le_{eff} and that it may be related to the unique properties of H_2 as a fuel compared with standard hydrocarbons. The authors also wish to emphasise that the unity exponent factor of Le_{eff} and the definition of Le_{eff} adopted in this work is simply empirically fitted to illustrate the point that thermo-diffusive properties need to be considered.

3.4 Effect of dilatation ratio

In this section, data is presented in which S_L was kept constant while ρ_u/ρ_b is varied. This was achieved by varying the equivalence ratio in CH_4-H_2 blends for varying H_2 volume fractions up to 100%, providing a range of ρ_u/ρ_b listed in Table 1. Experiments were conducted for both the 6- and 12-injector configurations and the results are plotted in Fig. 8. Fig. 8a shows that S_a increases with increasing H_2 content, despite a fixed S_L and a decreasing dilatation ratio. The direction of the trend is a surprising result given previous results with hydrocarbon fuels and detailed LES by Topperwein et al. [8] who demonstrated that a decrease in ρ_u/ρ_b is strongly correlated with a corresponding decrease, and not increase in S_a.

However, the LES also considered pure hydrocarbon fuel and not H_2 which has significantly different combustion properties that are likely responsible for the inverse trend. This result indicates that the effect of decreasing ρ_u/ρ_b is more than compensated by the high diffusivity of lean H_2 flames as well as the effect of wrinkling/turbulence on the propagation speed as found in the fan stirred bomb literature [27, 40, 41] and a recent DNS study by Rieth et al. [42]. In an effort to capture the thermo-diffusive effects, S_a is re-plotted in Fig. 8b against $(\rho_u/\rho_b)\cdot S_L \cdot Le_{eff}$, using Le_{eff} based on the heat release rate method. Here the mixtures get increasingly lean with increased H_2 content, resulting in $Le_{eff} << 1$. Despite the correction, the downward trend of S_a with varying ρ_u/ρ_b is only marginally flattened. This again suggests that the contribution of ρ_u/ρ_b in H_2 flames and blends is compensated by thermo-diffusive effects.

3.5 Geometric factors

Finally, the effect of injector spacing on the flame propagation speed during light around is considered.

Injector spacings of l_s/d_{inj} = 4.67 and 2.34, corresponding to the 6- and 12-injector configuration were investigated.

The choice of l_s/d_{inj} allows us to study the effect of flame proximity on the flame propagation speed during light-around noting that in the 6-injector case, adjacent injectors are sufficiently far apart compared to the 12-injector configuration as shown in Fig. 5. A recent study by [4] in a similar geometry considered 12 and 18 injectors with spacings of l_s/d_{inj} = 2.34 and 1.56 but found little change in the flame propagation speed. In these experiments the exit velocity of each injector was kept constant at U = 10 m/s.

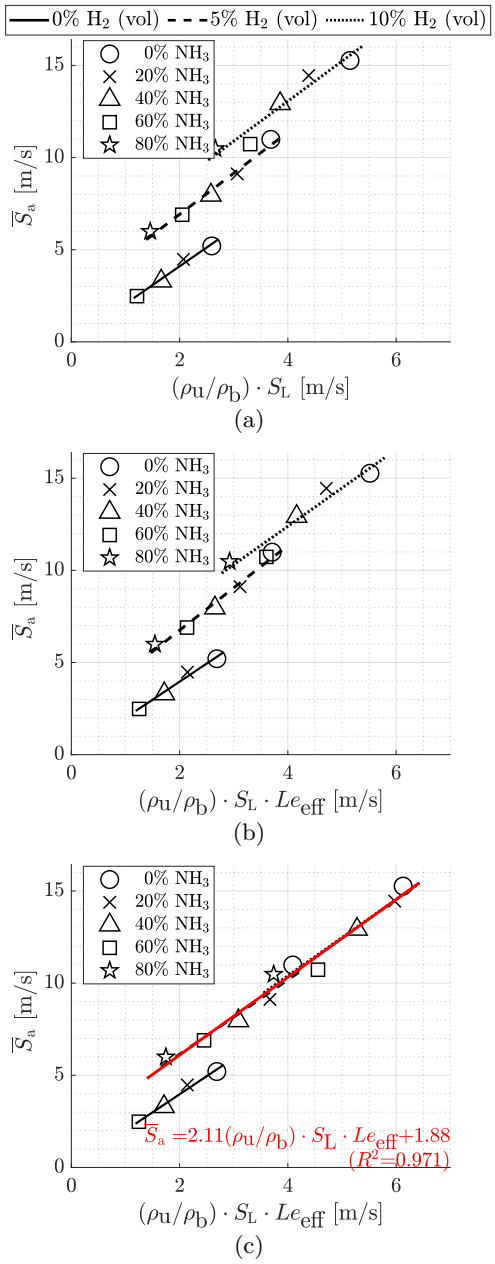

Figure 7: Light-around speeds of CH_4-NH_3 blends with different levels of H_2 enrichment. ρ_u/ρ_b is kept constant while S_L is varied. CH_4-H_2 blends refer to cases with 0% NH_3 and are denoted with '○'. (a): with no Le correction, (b) Le_{eff} based on volume weighting, (c) Le_{eff} based on heat release weighing. The Le_{eff} in all cases is ≥ 1.

The results are plotted in Fig. 9a and Fig. 9b for hydrocarbon fuels and CH_4-NH_3 blends with fixed ρ_u/ρ_b respectively. Since no H_2 was added in these experiments, no corrections for Le_{eff} were made. In both cases, a distinct increase in S_a in the 12-injector case is observed compared with the 6-injector case but all cases show a linear dependence of increasing S_a with an increase in the product of ρ_u/ρ_b and S_L. There is a notable difference in S_a between the hydrocarbons and the CH_4-NH_3 blends. In the case of the hydrocarbons, it is not possible to fix the ρ_u/ρ_b and vary S_L: both are varied together as a lumped parameter. For the hydrocarbon cases, the small but definite differences is not consistent with the findings of [4]. In CH_4-NH_3 blends where ρ_u/ρ_b is fixed, the magnitude of the variation of S_a with S_L is almost exactly double which suggests a scaling with power given that there are exactly half the number of injectors. To test this, a third plot (blue dotted line) representing the 12-injector cases of CH_4-NH_3 blends, whereby the total thermal power is matched with those of the 6-injector cases, is shown in Fig. 9b. It shows no collapse in the data noting that in this case, we have matched the total thermal power. Despite a reduction in injector exit velocity U by half (to match the total thermal power), the 12-injector cases still have higher S_a values. These discrepancies may arise from turbulence and flame interactions in the 12-injector configuration. This suggests that a number of factors such as a different injector spacing, a non-homogeneous volume of reactants at ignition, or different turbulence levels in the annulus can influence the ignition propagation speed.

4 Conclusions

This paper presented the effect of ammonia and hydrogen blends on ignition and light-around in a premixed annular combustor. In the first part of the paper, previous findings relating the dependence of flame propagation speed S_a on laminar flame speed for hydrocarbon fuels were corroborated. A lumped parameter, a product of dilatation ratio ρ_u/ρ_b and laminar flame speed S_L, was used to reflect the change in both the laminar flame speed and the dilatation ratio as equivalence ratio was varied, and a strong correlation was found between S_a and $(\rho_u/\rho_b)\cdot S_L$. This is consistent with past studies.

In the second part of the paper, CH_4-NH_3 blends were investigated for their impact on ignition dynamics. CH_4-NH_3 blends with varying NH_3 volume fractions were used to fix ρ_u/ρ_b while varying S_L. To maximise the range of S_L considered, volume fractions of H_2 were added at 5% or 10% of the total reactant flow volume. It was found that thermodiffusive effects significantly influence the flame propagation speed; applying an effective Lewis number computed based on the heat release-based approach results in good scaling for the cases with H_2 added to CH_4-NH_3 blends. However, it remains to be seen why blends without H_2 still exhibit an offset from those with H_2 added.

CH_4-H_2 blends were also considered in the current work. The equivalence ratio and H_2 volume fraction were varied to keep the laminar flame speed S_L constant with decreasing dilatation ratio ρ_u/ρ_b. Contrary to expectations, it was found that S_a increases with decreasing ρ_u/ρ_b. It is reasonable to expect that the high diffusivity of lean H_2 flames plays a major role in this surprising finding. Ongoing efforts are being made to explain this anomaly.

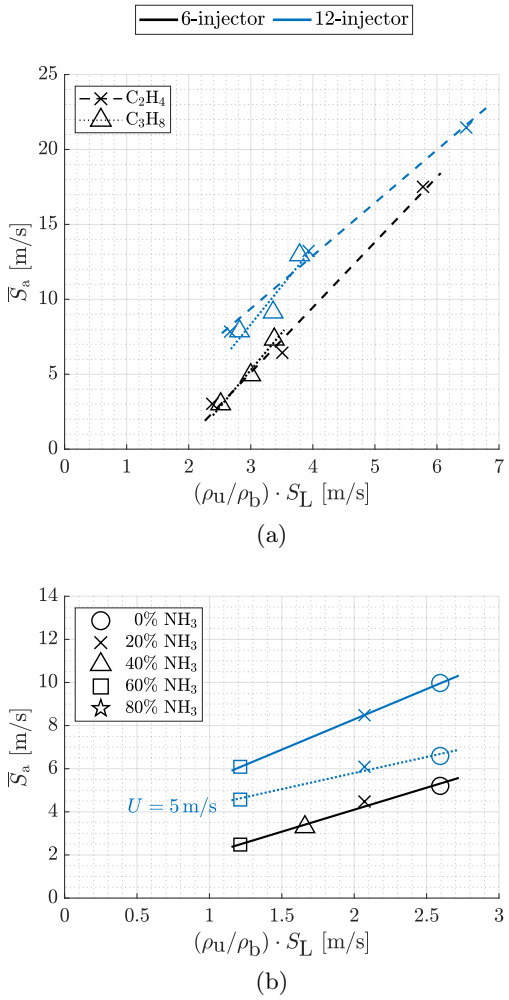

Figure 9: Plots showing the (a) light-around propagation speeds of hydrocarbon fuels (C_2H_4 and C_3H_8), and (b) light-around propagation speeds of CH_4-NH_3 fuel blends which have constant ρ_u/ρ_b while S_L is varied. In both the 6-injector (plotted in black) and 12-injector (in blue solid lines) cases, the exit velocity at each injector is kept constant at 10 m/s (constant thermal power per injector) and no Le_{eff} correction was applied as no H_2 was added. The blue dotted line represents 12-injector cases whereby the total thermal power (so exit velocity is reduced to 5 m/s) is matched with those of the 6-injector cases (black line).

Finally, the effect of injector spacing on hydrocarbon fuels, ammonia blends, and hydrogen blends was evaluated. It was found that in all cases, the 12-injector configuration always have faster propagation speeds. The difference in propagation speed was more distinct in the ammonia and hydrogen blends. Matching either the injector thermal power or total thermal power did not produce similar ignition propagation speeds, suggesting the role of turbulence, flame interaction, and fuel concentration at play.

In conclusion, current investigations on ammonia and hydrogen blends suggest that the unique thermodiffusive properties of H_2 plays a significant role in influencing the light-around of an annular combustor. Therefore, using hydrogen as an alternative fuel for decarbonisation requires careful consideration of the thermo-diffusive effects which can significantly modify ignition behaviour.

This project has received funding from the European Union's Horizon 2020 research and innovation program under Grant Agreement No 765998 (ANNULIGhT).

References

[1] Bourgouin, J.-F., Durox, D., Schuller, T., Beaunier, J., and Candel, S., 2013. "Ignition Dynamics of an Annular Combustor Equipped with Multiple Swirling Injectors". *Combustion and Flame,* ***160***(8), Aug., pp. 1398–1413.

[2] Prieur, K., Durox, D., Beaunier, J., Schuller, T., and Candel, S., 2017. "Ignition Dynamics in an Annular Combustor for Liquid Spray and Premixed Gaseous Injection". *Proceedings of the Combustion Institute,* ***36***(3), pp. 3717–3724.

[3] Xia, Y., Linghu, C., Zheng, Y., Ye, C., Ma, C., Ge, H., and Wang, G., 2019. "Experimental Investigation of the Flame Front Propagation Characteristic During Light-Round Ignition in an Annular Combustor". *Flow, Turbulence and Combustion,* ***103***(1), June, pp. 247–269.

[4] Ciardiello, R., de Oliveira, P. M., Skiba, A. W., Mastorakos, E., and Allison, P. M., 2020. "Effect of Spark Location and Laminar Flame Speed

on the Ignition Transient of a Premixed Annular Combustor". *Combustion and Flame,* ***221***, Nov., pp. 296–310.

[5] Ruetsch, G. R., and Broadwell, J. E., 1995. Effects of confinement on partially premixed flames. Annual Research Briefs, Centre for Turbulence Research, Stanford University.

[6] Barré, D., Esclapez, L., Cordier, M., Riber, E., Cuenot, B., Staffelbach, G., Renou, B., Vandel, A., Gicquel, L. Y., and Cabot, G., 2014. "Flame propagation in aeronautical swirled multi-burners: Experimental and numerical investigation". *Combustion and Flame,* ***161***(9), Sept., pp. 2387–2405.

[7] Machover, E., and Mastorakos, E., 2017. "Experimental Investigation on Spark Ignition of Annular Premixed Combustors". *Combustion and Flame,* ***178***, Apr., pp. 148–157.

[8] Töpperwien, K., Puggelli, S., and Vicquelin, R., 2022. "Analysis of flame propagation mechanisms during light-round in an annular spray flame combustor: the impact of wall heat transfer and two-phase flow". *Combustion and Flame,* ***241***, July, p. 112105.

[9] Lipatnikov, A. N., and Chomiak, J., 2002. "Turbulent flame speed and thickness: phenomenology, evaluation, and application in multi-dimensional simulations". *Progress in Energy and Combustion Science*, p. 74.

[10] Driscoll, J., 2008. "Turbulent premixed combustion: Flamelet structure and its effect on turbulent burning velocities". *Progress in Energy and Combustion Science,* ***34***(1), Feb., pp. 91–134.

[11] Bradley, D., Lau, A. K. C., Lawes, M., and Smith, F. T., 1992. "Flame stretch rate as a determinant of turbulent burning velocity". *Philosophical Transactions of the Royal Society of London. Series A: Physical and Engineering Sciences,* ***338***(1650), Feb., pp. 359–387. Publisher: Royal Society.

[12] Kobayashi, H., Seyama, K., Hagiwara, H., and Ogami, Y., 2005. "Burning velocity correlation of methane/air turbulent premixed flames at high pressure and high temperature". *Proceedings of the Combustion Institute,* ***30***(1), Jan., pp. 827–834.

[13] Zimont, V. L., 1979. "Theory of turbulent combustion of a homogeneous fuel mixture at high reynolds numbers". *Combustion, Explosion, and Shock Waves,* ***15***(3), pp. 305–311.

[14] Zhong, L., Yang, Y., Jin, T., Xia, Y., Fang, Y., Zheng, Y., and Wang, G., 2021. "Local flame and flow properties of propagating premixed turbulent flames during light-round process in a MICCA-type annular combustor". *Combustion and Flame,* ***231***, Sept., p. 111494.

[15] Mellor, A., 1990. *Design of Modern Turbine Combustors*. Academic Press.

[16] Candel, S., Durox, D., Schuller, T., Bourgouin, J.-F., and Moeck, J. P., 2014. "Dynamics of Swirling Flames". *Annual Review of Fluid Mechanics,* ***46***(1), Jan., pp. 147–173.

[17] Machover, E., and Mastorakos, E., 2016. "Spark Ignition of Annular Non-Premixed Combustors". *Experimental Thermal and Fluid Science,* ***73***, May, pp. 64–70.

[18] Worth, N. A., and Dawson, J. R., 2013. "Modal Dynamics of Self-Excited Azimuthal Instabilities in an Annular Combustion Chamber". *Combustion and Flame,* ***160***(11), Nov., pp. 2476–2489.

[19] Worth, N. A., and Dawson, J. R., 2013. "Self-Excited Circumferential Instabilities in a Model Annular Gas Turbine Combustor: Global Flame Dynamics". *Proceedings of the Combustion Institute,* ***34***(2), Jan., pp. 3127–3134.

[20] Kwah, Y. H., Agostinelli, P. W., Richard, S., Exilard, G., Pascaud, S., Gicquel, L., and Dawson, J. R., 2022. "Effect of Strong Azimuthal Swirl on Ignition and Light-Around in an Annular Combustor". *Journal of Engineering for Gas Turbines and Power,* ***144***(11), Nov., p. 111010.

[21] Philip, M., Boileau, M., Vicquelin, R., Schmitt, T., Durox, D., Bourgouin, J.-F., and Candel, S., 2014. "Simulation of the Ignition Process in an Annular Multiple-Injector Combustor and Comparison with Experiments". *Journal of Engineering for Gas Turbines and Power,* ***137***(3), Sept., p. 031501.

[22] Puggelli, S., Lancien, T., Prieur, K., Durox, D., Candel, S., and Vicquelin, R., 2020. "Impact of Wall Temperature in Large Eddy Simulation of Light-Round in an Annular Liquid Fueled Combustor and Assessment of Wall Models". *Journal of Engineering for Gas Turbines and Power,* ***142***(1), Jan., p. 011018.

[23] Hai Wang, and Alexander Laskin, 1998. A Comprehensive Kinetic Model of Ethylene and Acetylene Oxidation at High Temperatures. Progress Report, Department of Mechanical Engineering, University of Delaware.

[24] Qin, Z., Lissianski, V. V., Yang, H., Gardiner, W. C., Davis, S. G., and Wang, H., 2000. "Combustion chemistry of propane: A case study of detailed reaction mechanism optimization". *Proceedings of the Combustion Institute,* ***28***(2), Jan., pp. 1663–1669.

[25] Mechanical and Aerospace Engineering (Combustion Research), 2016. Chemical-Kinetic Mechanisms for Combustion Applications, Dec.

[26] Goodwin, D. G., Speth, R. L., Moffat, H. K., and Weber, B. W., 2018. Cantera: An Object-oriented Software Toolkit for Chemical Kinetics, Thermodynamics, and Transport Processes.

[27] Lipatnikov, A., and Chomiak, J., 2005. "Molecular transport effects on turbulent flame propagation and structure". *Progress in Energy and Combustion Science,* ***31***(1), Jan., pp. 1–73.

[28] Bouvet, N., Halter, F., Chauveau, C., and Yoon, Y., 2013. "On the effective Lewis number formulations for lean hydrogen/hydrocarbon/air mixtures". *International Journal of Hydrogen Energy,* ***38***(14), May, pp. 5949–5960.

[29] Muppala, S., Nakahara, M., Aluri, N., Kido, H., Wen, J., and Papalexandris, M., 2009. "Experimental and analytical investigation of the turbulent burning velocity of two-component fuel mixtures of hydrogen, methane and propane". *International Journal of Hydrogen Energy,* ***34***(22), Nov., pp. 9258–9265.

[30] Law, C., Jomaas, G., and Bechtold, J., 2005. "Cellular instabilities of expanding hydrogen/propane spherical flames at elevated pressures: theory and experiment". *Proceedings of the Combustion Institute,* ***30***(1), Jan., pp. 159–167.

[31] Vu, T. M., Park, J., Kwon, O. B., and Kim, J. S., 2009. "Effects of hydrocarbon addition on cellular instabilities in expanding syngas–air spherical premixed flames". *International Journal of Hydrogen Energy,* ***34***(16), Aug., pp. 6961–6969.

[32] Vu, T. M., Park, J., Kim, J. S., Kwon, O. B., Yun, J. H., and Keel, S. I., 2011. "Experimental study on cellular instabilities in hydrocarbon/hydrogen/carbon monoxide–air premixed flames". *International Journal of Hydrogen Energy,* ***36***(11), June, pp. 6914–6924.

[33] Joulin, G., and Mitani, T., 1981. "Linear stability analysis of two-reactant flames". *Combustion and Flame,* ***40***, Jan., pp. 235–246.

[34] Jackson, T. L., 1987. "Effect of Thermal Expansion on the Stability of Two-Reactant Flames". *Combustion Science and Technology,* ***53***(1), May, pp. 51–54.

[35] Beeckmann, J., Hesse, R., Kruse, S., Berens, A., Peters, N., Pitsch, H., and Matalon, M., 2017. "Propagation speed and stability of spherically expanding hydrogen/air flames: Experimental study and asymptotics". *Proceedings of the Combustion Institute,* ***36***(1), pp. 1531–1538.

[36] Peters, N., and Williams, F., 1987. "The asymptotic structure of stoichiometric methane-air flames". *Combustion and Flame,* ***68***(2), May, pp. 185–207.

[37] Bradley, D., Hicks, R., Lawes, M., Sheppard, C., and Woolley, R., 1998. "The Measurement of Laminar Burning Velocities and Markstein Numbers for Iso-octane–Air and Iso-octane–n-Heptane–Air Mixtures at Elevated Temperatures and Pressures in an Explosion Bomb". *Combustion and Flame,* ***115***(1-2), Oct., pp. 126–144.

[38] Lancien, T., Prieur, K., Durox, D., Candel, S., and Vicquelin, R., 2019. "Leading point behavior during the ignition of an annular combustor with liquid n-heptane injectors". *Proceedings of the Combustion Institute,* ***37***(4), pp. 5021–5029.

[39] Philip, M., Boileau, M., Vicquelin, R., Schmitt, T., Durox, D., Bourgouin, J.-F., and Candel, S., 2014. "Ignition Sequence of an Annular Multi-Injector Combustor". *Physics of Fluids,* ***26***(9), Sept., p. 091106.

[40] Karpov, V. P., and Severin, E. S., 1980. "Effects of molecular-transport coefficients on the rate of turbulent combustion". *Combustion, Explosion, and Shock Waves,* ***16***(1), pp. 41–46.

[41] Wu, M. S., Kwon, S., Driscoll, J. F., and Faeth, G. M., 1990. "Turbulent Premixed Hydrogen/Air Flames at High Reynolds Numbers". *Combustion Science and Technology,* ***73***(1-3), Sept., pp. 327–350.

[42] Rieth, M., Gruber, A., Williams, F. A., and Chen, J. H., 2022. "Enhanced burning rates in hydrogen-enriched turbulent premixed flames by diffusion of molecular and atomic hydrogen". *A dedication to Professor Kenneth Noel Corbett Bray,* ***239***, May, p. 111740.

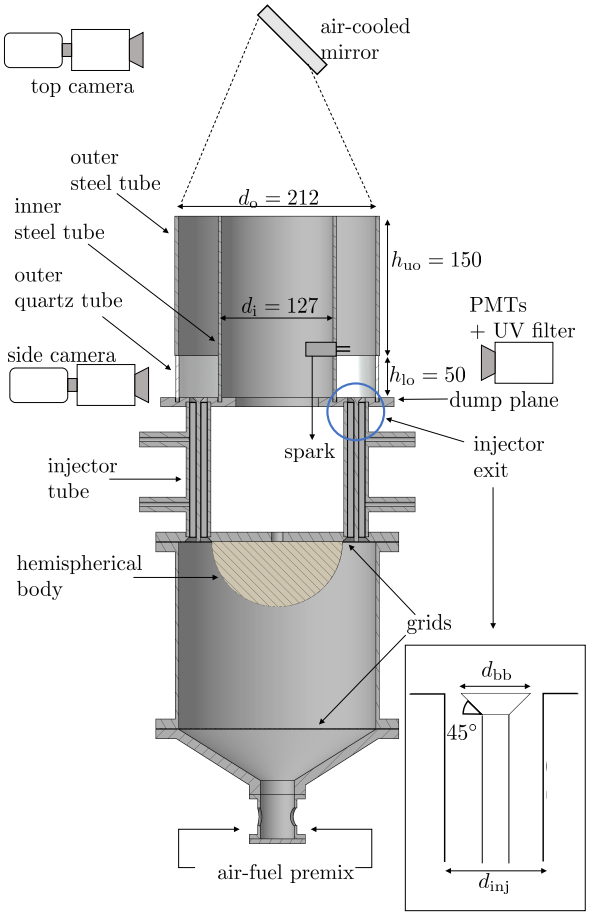

Figure 1: Schematic of the NTNU atmospheric annular combustor and the relevant diagnostics. Inset shows the injector with bluff body. Drawings not to scale to maximise readability.

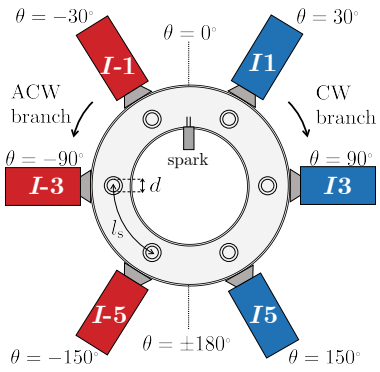

Figure 2: Schematic of the PMT positions around the annulus chamber for the detection of flames. Drawings not to scale to maximise readability.

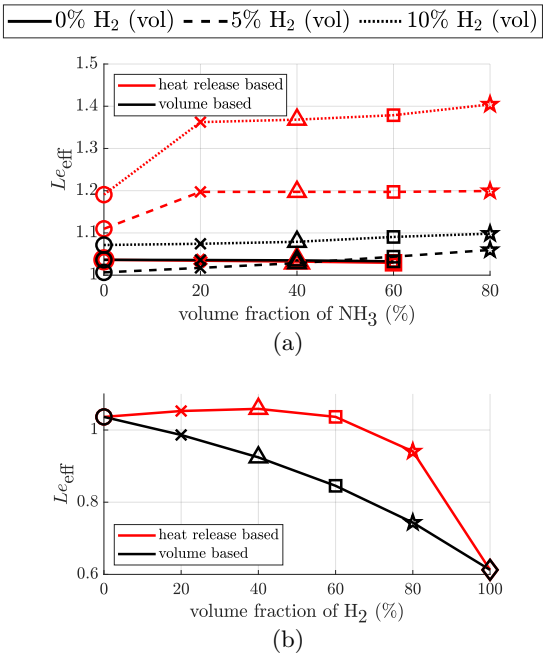

Figure 3: (a) Le_{eff} for CH_4-NH_3 blends at a fixed dilatation ratio ρ_u/ρ_b. The equivalence ratios of the blends are between 0.95 to 1.08. (b) Le_{eff} of CH_4-H_2 blends at a fixed laminar flame speed S_L = 0.34 m/s. The equivalence ratio of the blend decreases from ϕ=0.95 for 0% H_2 to ϕ=0.44 for 100% H_2. These computed values of Le_{eff} are used to compensate for the thermo-diffusive effects of the fuel blends in Fig. 7 and Fig. 8.

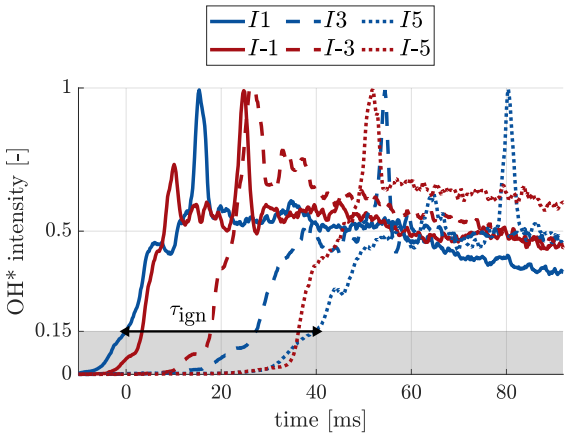

Figure 4: A typical time series of the light-around sequence characterised using PMTs. Injectors ignited by the CW flame branch are plotted in blue ($I1$, $I3$, $I5$), while those ignited by the ACW flame branch are plotted in red (I-1, I-3, I-5). The definition of light-around time, τ_{ign}, is based on a normalised threshold of 0.15.

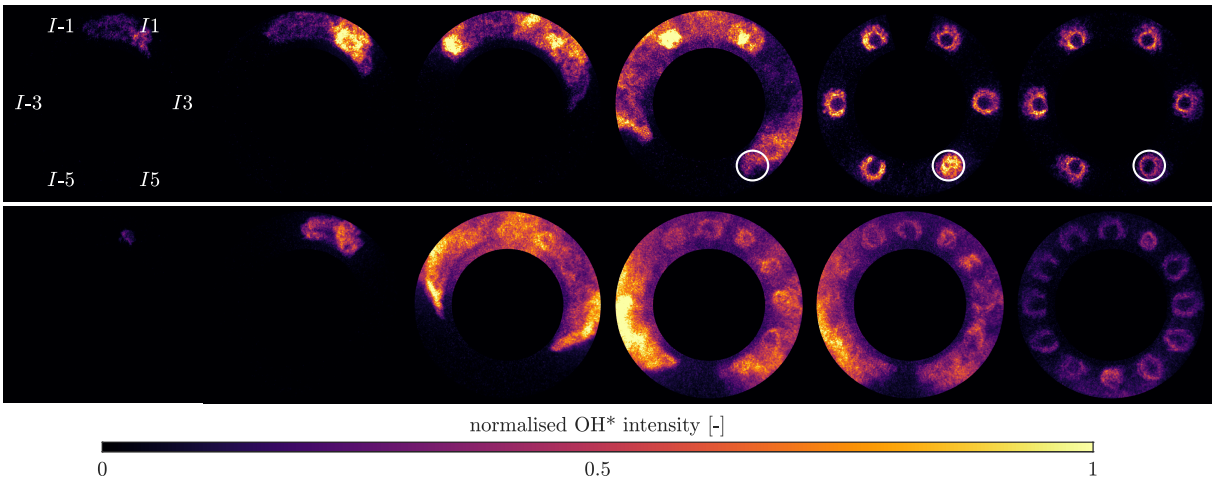

Figure 5: Example of an ignition sequence. In the last three images, $I5$ is circled in white. The image sequence shows the CW flame branch successfully propagating past $I5$ before reaching maximum OH* intensity after a certain time delay. The intensity eventually decreases and stabilises after the successful attachment and stabilisation on the bluff body.

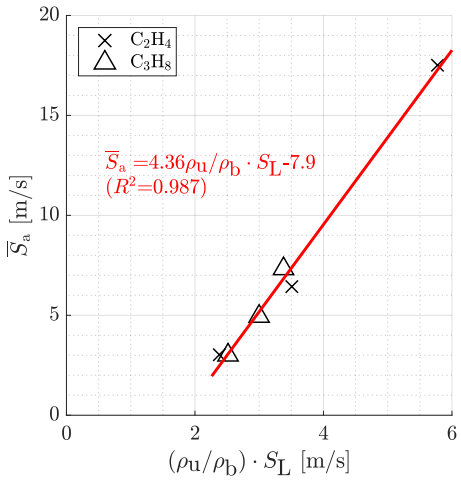

Figure 6: S_a against $(\rho_u/\rho_b) \cdot S_L$ for hydrocarbon fuels.

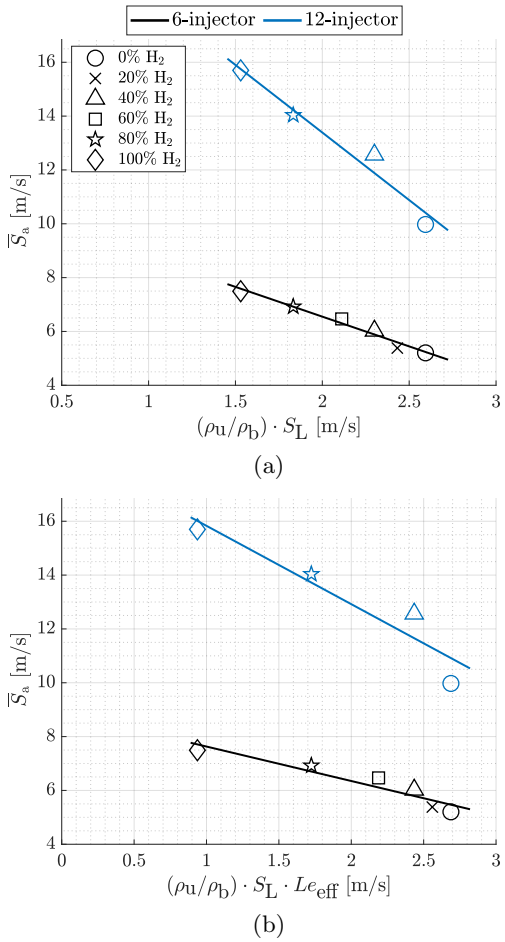

Figure 8: Light-around propagation speeds of CH_4-H_2 blends. S_L is kept constant while ρ_u/ρ_b is varied. (a) without Le_{eff} correction, and (b) with heat release mass-based Le_{eff} correction. In both the 6-injector (plotted in black) and 12-injector (in blue) cases, the exit velocity at each injector is kept constant at 10 m/s.